Collective polaritonic modes in an array of two-level quantum emitters coupled to an optical nanofiber

D. F. Kornovan,[1,2,*] A. S. Sheremet,[1,3] and M. I. Petrov[1,2,4]
[1]*ITMO University, Birzhevaya liniya 14, 199034 St. Petersburg*
[2]*St. Petersburg Academic University, 8/3 Khlopina str., 194021 St. Petersburg, Russia*
[3]*Russian Quantum Center, Novaya str. 100, 143025 Skolkovo, Moscow Region, Russia*
[4]*University of Eastern Finland, Yliopistokatu 7, FI-80101 Joensuu, Finland*
(Received 14 August 2016; revised manuscript received 22 November 2016; published 13 December 2016)

In this paper we develop a microscopic analysis of the light scattering on a periodic two-level atomic array coupled to an optical nanofiber. We extend the scattering matrix approach for two-level system interaction with nanofiber fundamental guided mode HE_{11}, which allows us to model the scattering spectra. We support these results by considering the dispersion of the polaritonic states formed by the superposition of the fundamental mode of light HE_{11} and the atomic chain states. To illustrate our approach we start by considering a simple model of light scattering over an atomic array in free space. We discuss Bragg diffraction in the atomic array and show that the scattering spectrum is defined by the nonsymmetric coupling of a two-level system with nanofiber and vacuum modes. The proposed method allows consideration of two-level system interactions with a full account of dipole-dipole interactions via both near fields and long-range interaction owing to nanofiber mode coupling.

DOI: 10.1103/PhysRevB.94.245416

I. INTRODUCTION

Controlling interactions of quantum emitters with optical nanostructures at the single-photon level is a key tool for the realization of quantum technologies [1,2]. Most experimental efforts focus on the reversible mapping of quantum states between light and matter and the implementation of quantum networking protocols using this interaction [3,4]. In this context localization of photonic modes at the nanoscale object opens a feasible route for on-chip quantum communication [5,6] and allows implementation of quantum networking protocols [7,8]. At the same time the evanescent character of the electromagnetic field manifested near a nano-object reveals fundamentally new features of light-matter interactions [9,10]. It is supported by the recent experimental progress in coupling single quantum sources to surface plasmon polaritons [11] and to photonic crystal waveguide modes [12], as well as by the results in neutral atoms trapped in the vicinity of an optical nanofiber [13–15]. The latter system is a versatile platform for achieving efficient light-atom coupling due to the collective nature of atomic interaction with an evanescent field of the single-photon mode [16]. This provides an exceptional opportunity to develop new approaches to the study of optical interactions of quantum many-body systems at the nanoscale level.

From this perspective the interaction between a two-level system and the evanescent field of the photonic mode yields to the formation of mixed polaritonic states with a modified dispersion relation [17,18]. Strong modification of dispersion is observed in a system of coupled plasmonic or dielectric resonators [19–22], which manifest themselves as classically coupled dipole-dipole particles. Nevertheless, considering the cold-atomic system trapped in the vicinity of an optical nanofiber the origin of the polaritonic states and their dispersion is significantly overlooked. The existing theoretical approaches are based on reflection and transmission spectroscopy of an incident fiber mode [23]. Theoretical predictions [24,25], and experimental verification [14] have shown that the spectral distribution of atomic fluorescence is strongly affected by the presence of the nanofiber. This has been experimentally examined [26,27] by detecting Bragg diffraction in the atomic chain. Despite its universality and technical convenience this approach does not clarify the exact picture of atom-atom interaction in the presence of a nanofiber, as it omits the exact details of dipole-dipole coupling. This paper aims to eliminate this gap by considering the eigenstates of the atomic array coupled to the nanofiber modes, which manifest themselves as polaritonic states. We apply the T-matrix method to study the scattering of the nanofiber mode over the constructed polaritonic states. Contrary to the reflectance and transmittance spectroscopy approach, this method can be universally extended to an arbitrary dense atomic array. In order to expose the full picture of the atom-photon interaction, we start our consideration with single-photon scattering at the atomic chain in vacuum and identifying the polaritonic states.

The paper is organized as follows: in Sec. II we describe in detail the theoretical approach to the considered problem in the case of an atomic chain in vacuum and in the vicinity of a nanofiber; in Sec. III we discuss the calculated scattering cross sections and interpret them using a polaritonic band diagram; and in Sec. IV we extend the approach to the case of the nanofiber and observe strong backscattering into the nanofiber mode when the Bragg condition is satisfied.

*newparadigm.dk@gmail.com

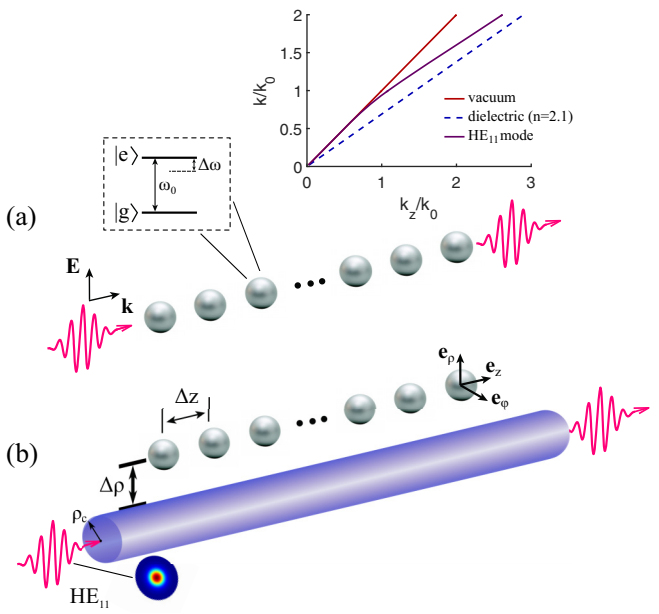

FIG. 1. Light scattering on the 1D array of two-level atoms with period Δz. (a) A single photon with the polarization vector parallel to the dipole moment of the atomic transition scatters and propagates along the atomic chain axis. (b) The scattering of a quasicircularly polarized single photon from the fundamental guided mode HE_{11} on the array of atoms trapped in the vicinity of the optical nanofiber. All atoms are positioned at the same distance $\Delta\rho$ from the fiber surface. Inset: Dispersion of a photon in vacuum (solid red line), dielectric with $n = 2.1$ (dashed blue line), and HE_{11} mode dispersion (solid purple line).

II. THEORETICAL APPROACH

We consider light scattering on a one-dimensional (1D) array of N two-level atoms with period Δz and compare this process for two systems: (i) the atomic chain in vacuum [see Fig. 1(a)] and (ii) the atomic chain in the vicinity of an optical silica nanofiber ($n = 2.1$) [see Fig. 1(b)]. In the first case we consider single-photon scattering with a wave vector directed along the atomic chain, and in the presence of a nanofiber we consider the propagation of a guided light field in the fundamental mode HE_{11} [Fig. 1(b)]. All atoms are placed at the same distance $\Delta\rho = 0.3\lambda_0$ from the fiber surface with radius $\rho_c = 0.25\lambda_0$, which is a typical value for such systems realized experimentally [15,28]. Here λ_0 is the wavelength of the atomic transition.

A. Interaction of a single photon with an atomic chain in a vacuum

In microscopic quantum theory the light scattering process can be described using the standard T-matrix formalism [29]. The total Hamiltonian $\hat{H}$ describing the interaction between propagating light and the atomic chain can be expanded as the sum of the nonperturbed part $\hat{H}_0$ and the interaction term $\hat{V}$ such that $\hat{H} = \hat{H}_0 + \hat{V}$, where

$$\hat{H}_0 = \sum_n \hbar\omega_0 \hat{\sigma}_n^+ \hat{\sigma}_n^- + \sum_\mu \hbar\omega_k \hat{a}_\mu^\dagger \hat{a}_\mu,$$
$$\hat{V} = -\sum_n \hat{\mathbf{d}}_n \hat{\mathbf{E}}(\mathbf{r}_n). \quad (1)$$

Here the interaction part of the Hamiltonian $\hat{V}$ is considered in the dipole approximation, where $\hat{\mathbf{d}}_n$ is the transition dipole moment operator of the nth atom, $\hat{\sigma}_n^+ = |e_n\rangle\langle g_n|$ and $\hat{\sigma}_n^- = |g_n\rangle\langle e_n|$ are raising and lowering atomic operators, $\hat{a}_\mu^\dagger$ ($\hat{a}_\mu$) are the bosonic creation (annihilation) operators, the index μ describes a particular field mode $\mu = (\mathbf{k},s)$, where $\mathbf{k}$ is the wave vector, $s = 1,2$ denotes two orthogonal polarizations, and $\hat{\mathbf{E}}(\mathbf{r}_n)$ is the total microscopic electric-field operator, which can be written as

$$\hat{\mathbf{E}}(\mathbf{r}) = \sum_\mu \sqrt{\frac{2\pi\hbar\omega_k}{\mathbb{V}}}(i\mathbf{e}_\mu \hat{a}_\mu e^{i\mathbf{kr}} + \text{H.c.}), \quad (2)$$

where $\mathbb{V}$ is the quantization volume and $\mathbf{e}_\mu$ is the unit polarization vector.

The T matrix then can be written in the form [29]

$$\hat{T} = \hat{V} + \hat{V}\hat{G}(E + i0)\hat{V}, \quad (3)$$

where $\hat{G}(z) = (z - \hat{H})^{-1}$ is the resolvent operator of the total Hamiltonian. In accordance with the rotating-wave approximation the matrix elements of the $\hat{T}$ operator can be found as a projection onto the Hilbert subspace of the vacuum state for the field subsystem and the single excited state for the atomic subsystem,

$$\hat{P}\hat{G}(E)\hat{P} = \hat{P}\,\frac{1}{E - \hat{H}_0 - \hat{\Sigma}(E)}\,\hat{P}, \quad (4)$$

where we have defined the projector operator as follows:

$$\hat{P} = \sum_{n=1}^{N} |g_1,\ldots,e_n,\ldots,g_N;\{0_\mu\}\rangle\langle\{0_\mu\};g_1,\ldots,e_n,\ldots,g_N|. \quad (5)$$

In Eq. (4) we introduced the level-shift operator $\hat{\Sigma}$ [29]. The form of this operator can be found as perturbative series in powers of $\hat{V}$.

At the lowest order of the perturbation theory the operator $\hat{\Sigma}$ can be described by two contributions corresponding to single-particle and the double-particle interactions [30]. The single-particle contribution leads to the Lamb shift and the finite lifetime of the atomic excited state, while the double-particle contribution is responsible for the excitation transfer between atoms.

Here we work in the resonant approximation, which allows consideration of the scattering of a photon with a carrier frequency ω close to the atomic transition frequency ω_0. In this approximation $\hat{\Sigma}(E)$ is assumed to be a slowly varying function of the argument so that $\hat{\Sigma}(E) \approx \hat{\Sigma}(E_0)$. The single- and

double-particle contributions can be written as

$$\Sigma^{(nn)}(E_0) = \hbar\left(\Delta_L - i\frac{\gamma_0}{2}\right),$$
$$\Sigma^{(mn)}(E_0) = -\mathbf{d}_m^*\left[\frac{e^{ikR}}{R}\left(\left(1+\frac{ikR-1}{k^2R^2}\right)\mathbf{I} + \frac{\mathbf{R}\otimes\mathbf{R}}{R^2}\cdot\frac{3-3ikR-k^2R^2}{k^2R^2}\right)\right]\mathbf{d}_n, \quad (6)$$

where Δ_L is the Lamb shift, γ_0 is the spontaneous emission rate, $k=\omega/c$ is the wave number of a vacuum photon, $R=|\mathbf{r_m}-\mathbf{r_n}|$ is the distance between atom m and atom n, $\mathbf{I}$ is the unit dyad, and $\otimes$ stands for the outer product.

Once the operator matrix $\hat{\Sigma}$ is computed we can construct the denominator in (4) and, by inverting it, obtain the matrix for the projected resolvent and the T matrix. We are interested in the scattering of the photon back into the same field mode, which is an elastic scattering channel, corresponding to the diagonal matrix element of the T matrix $T_{ii}(E)$.

In the case of a vacuum, this matrix element is connected to the total scattering cross section according to the optical theorem [30,31]: $\sigma_{\text{tot}}(E)\sim \text{Im}T_{ii}(E)$. In the presence of a nanofiber this exact formula for the total scattering cross section is not applicable. We introduce the quantity, which shows the enhancement of the scattered energy in a chain of N atoms, compared to the maximal energy scattered on a single atom,

$$\sigma_N(E) = \frac{\text{Im}\ T_{ii}^{(N)}(E)}{\text{Im}\ T_{ii}^{(1)}(E_{\text{res}})}, \quad (7)$$

where $\text{Im}T_{ii}^{(1)}(E_{\text{res}})$ corresponds to a resonant value of the T matrix for a single photon scattering off a single atom.

B. Interaction of a guided light with an atomic chain in the presence of a nanofiber

However, to correctly take into account the optical fiber we need to modify the approach discussed in Sec. II A, and we do this in two steps. First, we need to modify the "outer" operators $\hat{V}$ in Eq. (3), which are responsible for the absorption of the incoming guided photon and emission of the photon back into the same field mode. To describe the field subsystem at this step we use the quantization scheme proposed in [32], where the quantized electric field of the guided mode of the nanofiber can be written as

$$\hat{\mathbf{E}}(\mathbf{r}) = \sum_\mu \mathbf{E}_\mu(\mathbf{r})\hat{a}_\mu + \text{H.c.}, \quad (8)$$

where $\mathbf{E}_\mu$ is the electric field of the guided mode μ:

$$\mathbf{E}_\mu(\mathbf{r}) = i\sqrt{\frac{2\pi\hbar\omega_\mu}{\mathbb{L}}}\tilde{\mathbf{E}}_\mu(\rho,\phi)e^{if\beta_\mu z+im\phi}. \quad (9)$$

Here β_μ is the propagation constant, $\tilde{\mathbf{E}}_\mu(\rho,\phi)$ is the amplitude of the electric field, $\mathbb{L}$ is the quantization length, the index $\mu=(\beta_l,f,m)$ describes a particular guided mode, and f and m define the direction of propagation $(+1/-1)$ and the mode angular momentum $(+1/-1)$, respectively. The electric field is periodic in the z direction and the periodicity condition can be written as $\beta_l\mathbb{L}=2\pi l$, where l is a positive integer number. The electric-field amplitude is normalized according to

$$\int_0^{2\pi}\int_0^\infty |\tilde{\mathbf{E}}_\mu(\rho,\phi)|^2 d\phi\rho d\rho = 1. \quad (10)$$

At the next step, we need to calculate the matrix elements of the operator $\hat{\Sigma}$ in the presence of a nanofiber. To account for the excitation transfer between atoms through the radiation of vacuum modes and modes of the nanofiber, we need to introduce the proper quantum-electrodynamical description of the electromagnetic field, which was developed by Welsch *et al.* in Ref. [33]. Using this formalism we can modify Hamiltonian (1) to describe our system as

$$\hat{H}_0 = \sum_n \hbar\omega_0\hat{\sigma}_n^+\hat{\sigma}_n^- + \int d\mathbf{r}'\int_0^\infty d\omega'\hbar\omega'\hat{\mathbf{f}}^\dagger(\mathbf{r}',\omega')\hat{\mathbf{f}}(\mathbf{r}',\omega'),$$
$$\hat{V} = -\sum_n \hat{\mathbf{d}}_n\hat{\mathbf{E}}(\mathbf{r}_n), \quad (11)$$

where ω_0 is the atomic transition frequency, $\hat{\mathbf{E}}(\mathbf{r}_n)$ is the total electric field, and $\hat{\mathbf{f}}(\mathbf{r}'\omega')$ and $\hat{\mathbf{f}}^\dagger(\mathbf{r}',\omega')$ are the bosonic vector local-field operators, which obey the following commutation relations:

$$[\hat{f}_i(\mathbf{r}',\omega'),\hat{f}_k^\dagger(\mathbf{r},\omega)] = \delta_{ik}\delta(\mathbf{r}'-\mathbf{r})\delta(\omega'-\omega),$$
$$[\hat{f}_i(\mathbf{r}',\omega'),\hat{f}_k(\mathbf{r},\omega)] = 0. \quad (12)$$

The positive-frequency part of the total electric field has the form

$$\hat{\mathbf{E}}^+(\mathbf{r}) = i\sqrt{4\hbar}\int d\mathbf{r}'\int_0^\infty d\omega'\frac{\omega'^2}{c^2}\sqrt{\varepsilon_I(\mathbf{r}',\omega')} \times \mathbf{G}(\mathbf{r},\mathbf{r}',\omega')\hat{\mathbf{f}}(\mathbf{r}',\omega'), \quad (13)$$

where $\varepsilon_I(\mathbf{r}',\omega')$ is the imaginary part of the dielectric permittivity of the media and $\mathbf{G}(\mathbf{r},\mathbf{r}',\omega')$ is the classical Green's tensor of the electric field. In the presence of the optical fiber the Green's tensor can be expanded into

$$\mathbf{G}(\mathbf{r},\mathbf{r}',\omega) = \mathbf{G}_0(\mathbf{r},\mathbf{r}',\omega) + \mathbf{G}_s(\mathbf{r},\mathbf{r}',\omega), \quad (14)$$

where $\mathbf{G}_0$ is the vacuum Green's tensor and $\mathbf{G}_s$ is the Green's tensor corresponding to the light scattering from the fiber. The scattering term of the Green's tensor can be expanded into the vector wave functions (WVFs), and the details of these calculations are given in the Appendix. At the lowest nonvanishing order the matrix elements of the level-shift operator in this case can be written as

$$\langle f|\hat{\Sigma}(E)|i\rangle = \sum_{|\alpha\rangle,|\beta\rangle}\langle f|\hat{V}|\alpha\rangle\langle\alpha|\frac{1}{E-\hat{H}_0+i\eta}|\beta\rangle\langle\beta|\hat{V}|i\rangle, \quad (15)$$

where $|i\rangle$ and $|f\rangle$ are the initial and final states of the system, respectively, $|\alpha\rangle$ and $|\beta\rangle$ are the two possible intermediate states with a single elementary excitation for the field subsystem, and both atoms are in either the excited or the ground state:

$$|e_n,e_m\rangle\times\hat{\mathbf{f}}^\dagger(\mathbf{r}',\omega')|\{0\}\rangle,$$
$$|g_n,g_m\rangle\times\hat{\mathbf{f}}^\dagger(\mathbf{r}',\omega')|\{0\}\rangle. \quad (16)$$

The derivation of these matrix elements of the level-shift operator can be found elsewhere [34,35] and here we provide only the final expression:

$$\langle f|\hat{\Sigma}(E)|i\rangle = -4\pi\frac{\omega_0^2}{c^2}\mathbf{d}_m^*\mathbf{G}(\mathbf{r}_m,\mathbf{r}_n,\omega_0)\mathbf{d}_n. \quad (17)$$

We should note that in the case of a single-particle contribution, where $|i\rangle = |f\rangle$ and, thus, $\mathbf{r}_n = \mathbf{r}_m$, the homogeneous part of the Green's function has a singularity in the real part $\mathrm{Re}[\mathbf{G}_0(\mathbf{r}_n,\mathbf{r}_n,\omega_0)] \to \infty$ which corresponds to the infinite Lamb shift due to the interaction with the vacuum modes. This term is renormalized and can be thought of as already incorporated into the definition of the transition frequency of atomic dipoles ω_0. However, $\mathrm{Re}[\mathbf{G}_s(\mathbf{r}_n,\mathbf{r}_n,\omega_0)]$ is finite and it leads to the presence of a Lamb shift due to the interaction of the excited atom with the fiber modes.

Now using (17) we can find the matrix $\Sigma(E)$, the T-matrix elements, and, consequently, the normalized scattering losses $\sigma_N(E)$. In this case when calculating the denominator of Eq. (7) the atom is placed at the same distance $\Delta\rho$ from the fiber surface as atoms in our periodic chain. Also, we note that E_{res} now differs from $\hbar\omega_0$ because of the Lamb shift.

III. RESULTS: ATOMIC CHAIN IN A VACUUM

We consider photon scattering in an atomic chain in vacuum in the geometry shown in Fig. 1(a). In this case we assume that the dipole moments of the atoms are aligned parallel to photon polarization.

We have applied the T-matrix approach to plot the spectra of the scattering cross section for different interatomic distances. The scattering intensity is shown in Fig. 2. One can note that it changes in a nonmonotonous way as the distance between the atoms varies. The most pronounced changes are observed when the period is approximately $m\lambda_0/2$, where m is an integer. For instance, changing the interatomic distance from $\Delta z = 0.49\lambda_0$ to $\Delta z = 0.55\lambda_0$ results in a decrease in the intensity and a widening of the peak. A similar but much weaker effect is observed when the distance is changed from $0.95\lambda_0$ to $1.05\lambda_0$. This behavior is related to the opening of the diffraction channels each time the Bragg condition is satisfied. On the other hand, this process can be easily understood by analyzing the eigenstates of the atomic system, which manifest themselves in polaritonic states.

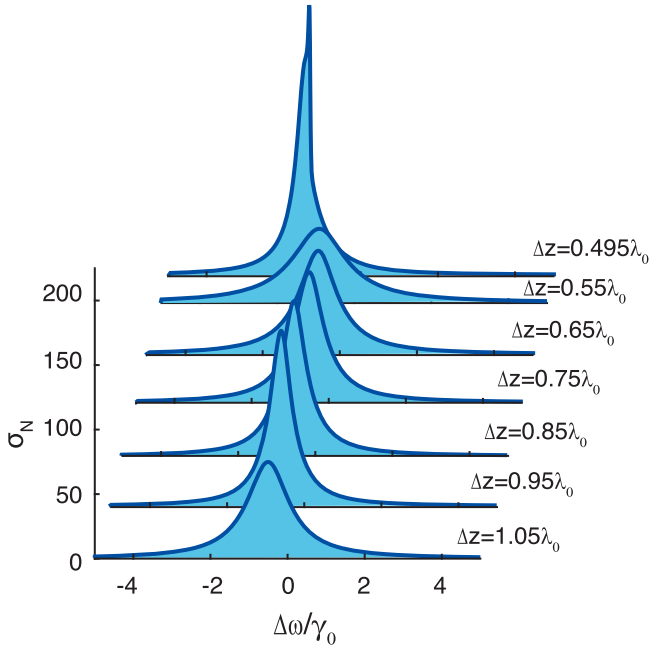

FIG. 2. Normalized total scattering cross section's dependence on photon frequency detuning $\Delta\omega = \omega - \omega_0$ for different periods of chain Δz in vacuum. The dipole transition is oriented parallel to the field polarization $\mathbf{d}||\mathbf{E}$. The number of atoms is $N = 100$.

A. Polaritonic states in an atomic chain

Polaritonic states can be constructed by defining the eigenstates of the level-shift operator, which is, in our approximation, the operator of dipole-dipole atomic coupling. In the limit of resonant excitation the eigenproblem can be formulated as follows:

$$\Sigma(\omega_0)\mathbf{v} = \mathcal{E}\mathbf{v}. \quad (18)$$

Here $\Sigma(\omega_0)$ is the matrix representation of the level-shift operator. The solution of this equation gives us N complex eigenvalues $\mathcal{E}_i = \hbar\omega_i$ and column eigenvectors $\mathbf{v}_i$, which are the energies and eigenstates of the system described in the basis of states with a single atomic excitation. We utilize the solution of a finite eigensystem to plot the dispersion curve for an infinite chain [19,36]. A problem of this type was also considered for one- and two-dimensional structures with excitons in [37], but formulated in a self-consistent way, where the energy dependence of $\Sigma(\omega)$ is kept. In our case, we calculate $\Sigma(\omega)$ at frequency ω_0, which is a simplification giving adequate results [4,36].

For this we correlate the eigenvector with the corresponding wave number k_z enumerating the eigenstates in accordance with the number of nodes l in the profile of the eigenmode $\mathbf{v_i}$. Then we can assign the corresponding wave number k_z to each mode according to

$$\frac{k_z^{(l)}}{K} = \frac{(l+1)}{2N}, \quad (19)$$

where $K = 2\pi/\Delta z$ is the reciprocal lattice vector of a periodic chain and $l = 0,1,2,\ldots$ is the mode number. For $l = 0$ relation (19) gives $\lambda_l = 2Nd$, so there is a single antinode in the profile of this fundamental mode, while for $l = N-1$ we have $\lambda_l = 2d$, and therefore, the neighboring atoms are exactly out of phase for this mode.

This procedure allows us to plot both the real and the imaginary parts of the eigenfrequencies of our system as functions of k_z, where the real part accounts for the dispersion of normal modes and the imaginary part describes radiative losses or the inverse lifetimes of the eigenstates.

In order to support the scattering cross-section spectra shown in Fig. 2 we illustrate the light interaction with the atomic chain by plotting the dispersion curves for transversal ($\mathbf{d} \perp \mathbf{e_z}$) polaritonic states (see Fig. 3). We consider subdiffractional ($K > 2k_0$) [Fig. 3(a)] and diffractional ($K < 2k_0$) [Fig. 4(b)] regimes, where the first Bragg condition is satisfied. The light line, which is vertical on the scale of the polaritonic bandwidth as $\gamma_0 \ll \omega_0$, divides the states into radiative and

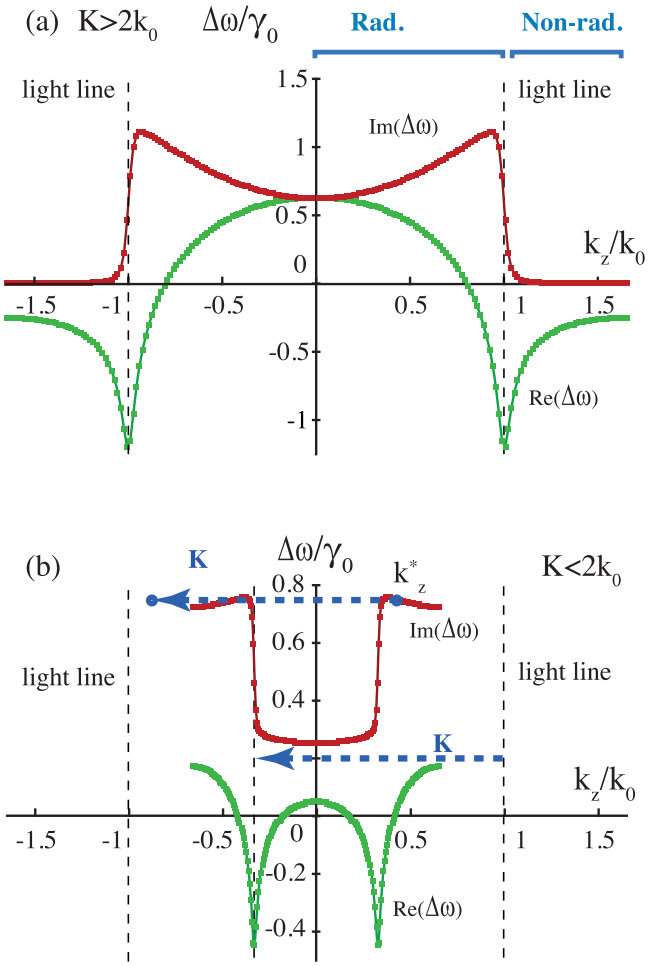

FIG. 3. Real (green curve) and imaginary (red curve) parts of the eigenfrequencies of the transversal polaritonic states with $\mathbf{d} \perp \mathbf{e_z}$ versus the corresponding k_z values for (a) the sub-diffractional case $K > 2k_0$ ($\Delta z = 0.3\lambda_0$) and (b) the diffractional case $K < 2k_0$ ($\Delta z = 0.75\lambda_0$). The dispersions of the vacuum photon modes (light line) are shown by dashed horizontal lines. Regions of radiative and nonradiative states are marked.

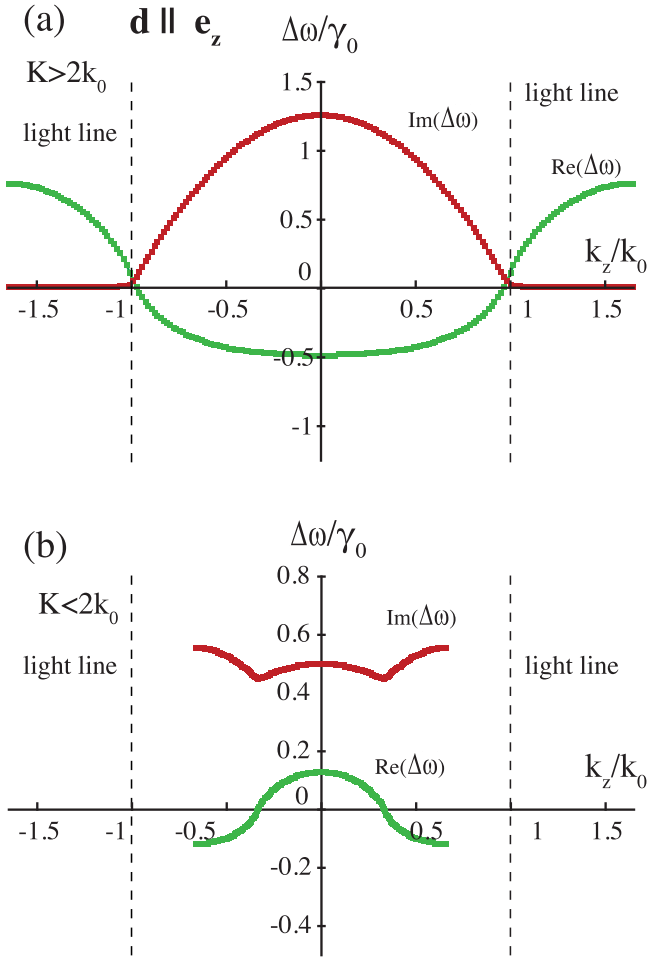

FIG. 4. Real (green curve) and imaginary (red curve) parts of the eigenfrequencies of the longitudinal polaritonic states with $\mathbf{d} \parallel \mathbf{e_z}$ versus the corresponding k_z values for (a) the subdiffractional case $K > 2k_0$ ($\Delta z = 0.3\lambda_0$) and (b) the diffractional case $K < 2k_0$ ($\Delta z = 0.75\lambda_0$). The dispersions of the vacuum photon modes (light line) are shown by dashed horizontal lines.

nonradiative ones. In the vicinity of point $k_z = k_0$ the atomic states undergo hybridization with vacuum photon modes. For the diffractional case [see Fig. 3(b)], all the eigenmodes become radiative as they appear above the light line. However, one should note that hybridization features are preserved but are shifted from the light line for quantity K, as the wave vector k_z is a quasivector of the polaritonic state and is conserved up to a reciprocal vector. Moreover, states near the band edges ($k_z > K - k_0$) become more radiative than states in the band center, as they have two channels of radiation: they can emit (i) a photon with $k_z^{\mathrm{ph}} = k_z^*$ and (ii) a photon with $k_z^{\mathrm{ph}} = k_z^* - K$.

The dispersion of the longitudinal modes ($\mathbf{d} \parallel \mathbf{e_z}$), similarly to the transversal modes, can also be divided into radiative and nonradiative regions (see Fig. 4). However, hybridization with the vacuum modes in the vicinity of the light line is not observed due to polarization mismatch: the vacuum modes have transversal polarization and the polaritonic excitations are longitudinal.

B. Bragg diffraction

The plotted dispersion curves clarify the character of the cross-section spectra shown in Fig. 2, in particular, the opening of the first Bragg diffraction channel when the period changes from $\Delta z = 0.49\lambda_0$ to $\Delta z = 0.51\lambda_0$. The k_z component of the incident photon equals k_0 according to Fig. 1(a), and for the subdiffractional regime the scattering occurs on states near the light line $k_z \approx k_0$ [see Fig. 5(b)]. In the subdiffractional regime, when $k_0 \lesssim K/2$ these states have low losses, which generates a narrow cross-section spectrum shape [see solid line in Fig. 5(a)]. After switching to the diffractional regime $k_0 \gtrsim K/2$ the incident photon scatters off states with $k_z = k_0 - K$ (umklapp process) as shown in Fig. 5(c). Due to the high radiative losses connected to free-space diffraction the cross-section spectrum is wide [see dashed line in Fig. 5(a)].

IV. RESULTS: ATOMIC CHAIN IN THE VICINITY OF AN OPTICAL NANOFIBER

The presence of an optical nanofiber changes the character of atomic interaction and allows long-range dipole-dipole

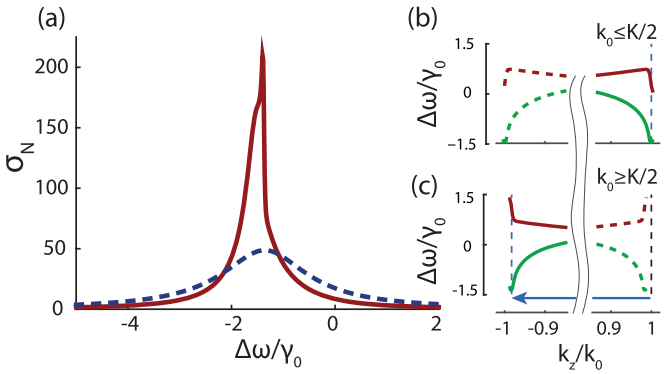

FIG. 5. Illustration of the diffraction channel opening in the photon scattering on a two-level atomic array in vacuum. (a) Scattering cross sections for two chain periods: $K \gtrsim 2k_0$ ($\Delta z = 0.49\lambda_0$) (solid red line) and $K \lesssim 2k_0$ ($\Delta z = 0.51\lambda_0$) (dashed blue line). (b, c) Dispersion curves (green) and inverse lifetimes (red curves) of these states in the region close to the situations shown in (a). The number of atoms is $N = 100$.

coupling between atoms not only via the vacuum, but also through the guided mode. To study this effect and its influence on the scattering of the guided mode over an atomic chain, we have applied the T-matrix method. In contrast to the commonly used transfer matrix method, where the interaction of the guiding mode with each atom is treated individually [26,38], here we consider the scattering on collective polaritonic states taking account of the full atomic dipole-dipole interaction and splitting their energy levels. For this we start by building the eigenstate picture of the atomic system with an optical nanofiber.

A. Dispersion of polaritonic states

The polaritonic dispersion relation in the presence of an optical nanofiber can be found from the eigenstates of the system, (18), but with the corrected level-shift operator, which includes interaction with the nanofiber by means of the scattering Green's function in Eq. (14). The real and imaginary parts of eigenfrequencies versus the corresponding k_z values are plotted in Fig. 6 for transverse $\mathbf{d} \parallel \mathbf{e}_\rho$ modes. The parameters of the nanofiber are chosen in such a way that it supports only one fundamental mode HE_{11} at the frequency of the atomic transition ω_0. The fiber mode dispersion curve is shown by the dash-dotted line in Fig. 6, in addition to the vacuum photon line, shown by the dashed line. In the subdiffractional regime $K > 2k_0$ the nanofiber interaction channel gives an anticrossing-like feature in the polaritonic dispersion in the vicinity of $k_z = k_0^f$, where k_0^f denotes the wave vector of the wave guiding photon having frequency ω_0. The nanofiber modifies the nonradiative atomic states and forms nanofiber coupled polaritonic states [see Fig. 6(a)]. These states are situated close to radiative states as the wave vector of the fundamental guided mode is close to the wave vector of the vacuum photon $|k_0 - k_0^f| \ll k_0$ (see Fig. 1). The peak in the spectrum of the imaginary frequency at $k_z = k_0^f$ is related to the leakage of the state through the fiber mode. For the diffractional regime $K < 2k_0$ [see Fig. 6(b)], all states

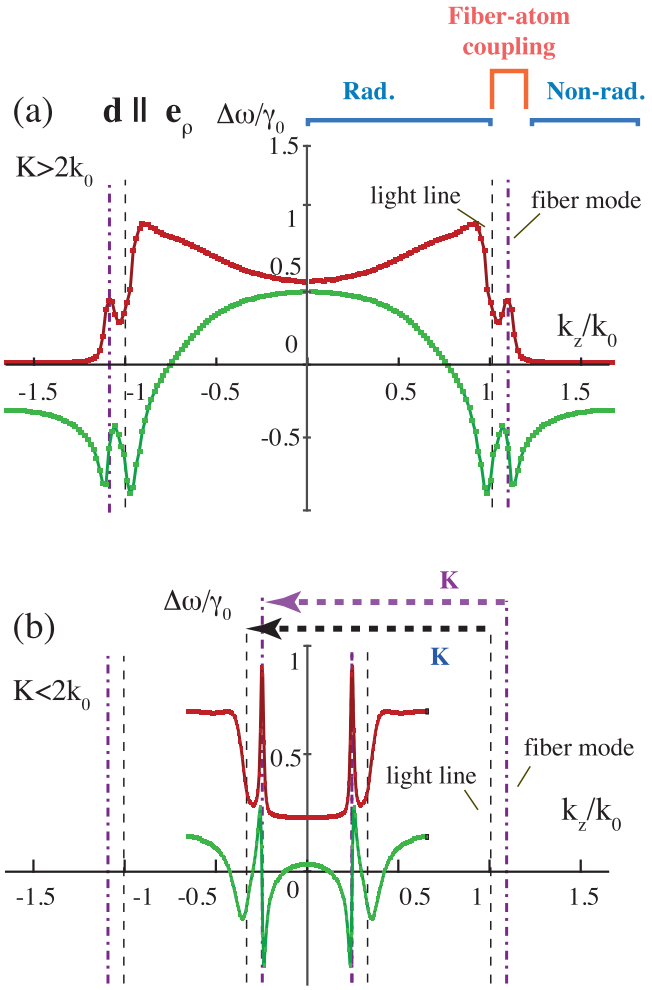

FIG. 6. Real (green curve) and imaginary (red curve) parts of the eigenfrequencies of the transversal polaritonic states with $\mathbf{d} \parallel \mathbf{e}_\rho$ versus the corresponding k_z values for (a) the subdiffractional case $K > 2k_0$ ($\Delta z = 0.3\lambda_0$) and (b) the diffractional case $K < 2k_0$ ($\Delta z = 0.75\lambda_0$). The dispersion of vacuum photon modes (light line) are shown by dashed black lines. The dispersion of the nanofiber fundamental mode HE_{11} is shown by the dash-dotted purple line. Regions of radiative, nonradiative, and strong coupling to the nanofiber mode states are shown. The number of atoms is $N = 100$, the nanofiber radius is $\rho_c = \lambda_0/4$, and the distance from the fiber surface is $\Delta\rho = 0.3\lambda_0$.

become radiative and there is resonant anticrossing coupling to the guided mode of the fiber at $\pm k_0^f \mp K$ along with the vacuum mode coupling at $\pm k_0 \mp K$.

The field of the fundamental fiber mode HE_{11} has all three components of the electric field, thus, in general all of them contribute to the dipole-dipole interaction. For completeness of consideration we have plotted the other two polarizations of the dipole moments of the atomic transition: the azimuthal transversal ($\mathbf{d} \parallel \mathbf{e}_\varphi$) and longitudinal ($\mathbf{d} \parallel \mathbf{e}_z$) polarizations are shown in Fig. 7. The dispersion of azimuthal modes is similar to that of radial modes but has a weaker interaction with the fiber mode due to the weaker amplitude of the azimuthal component of the electrical field in the fiber mode. The longitudinal modes fully resemble the longitudinal modes in

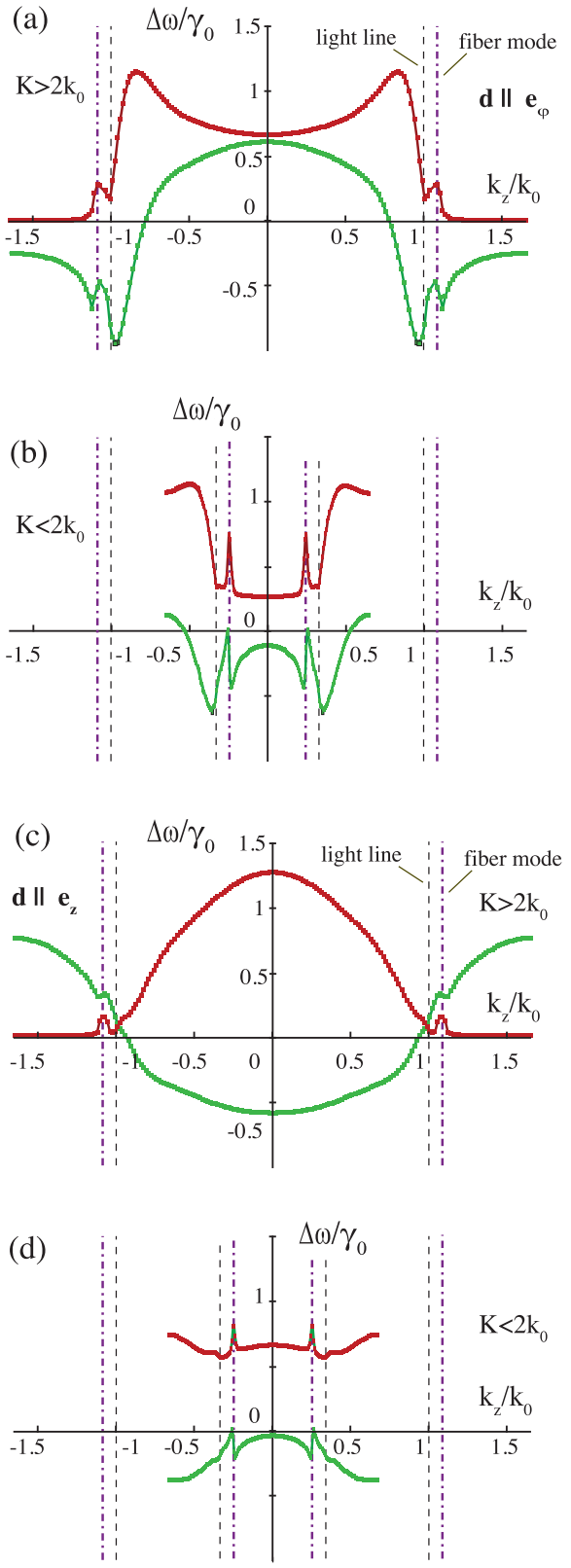

FIG. 7. Real (green curve) and imaginary (red curve) parts of the eigenfrequencies of transversal polaritonic states with $\mathbf{d} \parallel \mathbf{e}_\varphi$ (a, b) and longitudinal states with $\mathbf{d} \parallel \mathbf{e_z}$ (c, d) versus the corresponding k_z values. (a, c) Subdiffractional case $K > 2k_0$ ($\Delta z = 0.3\lambda_0$); (b, d) diffractional case $K < 2k_0$ ($\Delta z = 0.75\lambda_0$). Parameters and notation are the same as in Fig. 6.

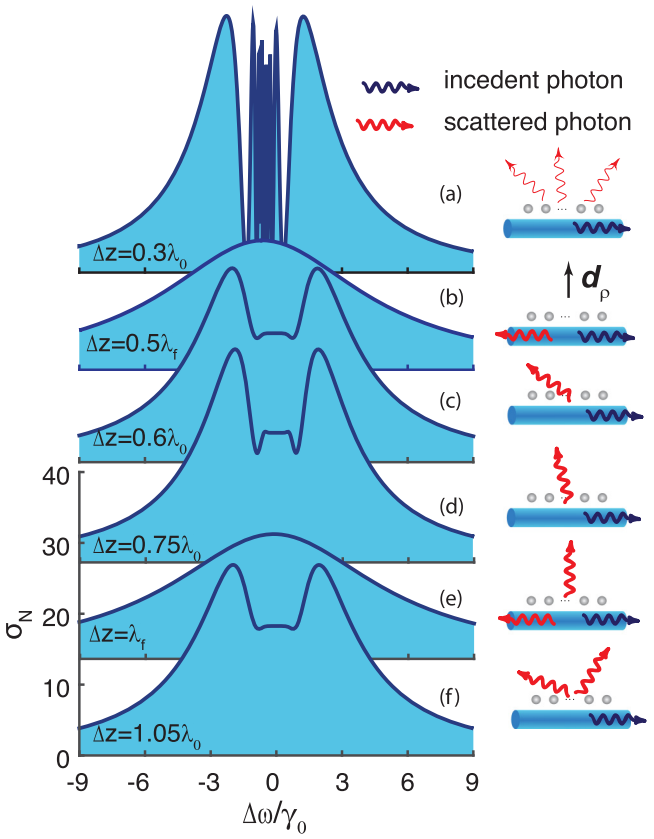

FIG. 8. Normalized scattering loss spectra of a two-level atomic chain consisting of $N = 200$ atoms in the vicinity of the nanofiber for different periods Δz: (a) $0.3\lambda_0$, (b) $0.5\lambda_f$, (c) $0.6\lambda_0$, (d) $0.75\lambda_0$, (e) λ_f, and (f) $1.05\lambda_0$. The nanofiber radius is $\rho_c = \lambda_0/4$, and the distance from the fiber surface is $\Delta\rho = 0.3\lambda_0$.

vacuum, with the fiber mode interaction being weaker than for the transversal modes. However, there is no coupling of atoms with the vacuum field due to polarization mismatch, but atoms are interacting with the fiber mode [see Figs. 7(c) and 7(d)], as the HE_{11} mode is not fully transversal and has a nonzero z component of the electric field, which makes its contribution to the interaction constant.

B. Fiber-mode scattering

We have analyzed the scattering of the fundamental fiber mode HE_{11} by the atomic chain in subdiffractional and diffractional regimes as shown in Fig. 8. We consider all atoms having only the $\mathbf{d}_\rho$ component of dipole transition matrix elements, which corresponds to Fig. 6. The presence of the nanofiber makes the system effectively 1D, which leads to significant changes in the normalized scattering loss spectra compared to the vacuum case. We plot the normalized scattering loss, (7), spectrum, which corresponds to the probability of a single photon's escaping from the guided mode after interaction with the atomic chain.

One can see in Fig. 8 that for the subdiffractional regime the spectrum is modulated by sharp resonances in the vicinity of the atomic resonant frequency ω_0. These resonances correspond to scattering on states with $k_z \approx k_f$ having low

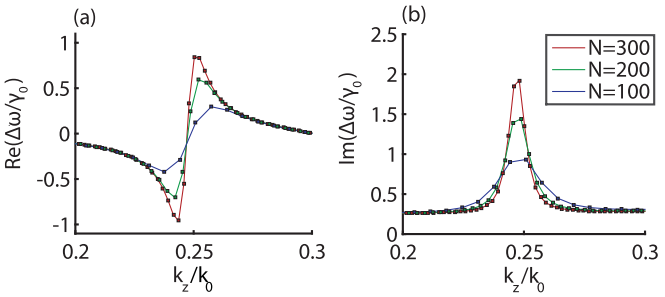

FIG. 9. (a) Real and (b) imaginary parts of eigenfrequencies for the transverse collective modes ($\mathbf{d}||\mathbf{e}_\rho$) versus k_z for a chain with period $\Delta z = 0.75\lambda_0$ and a varying number of atoms N. The nanofiber radius is $\rho_c = \lambda_0/4$, and the distance from the fiber surface is $\Delta\rho = 0.3\lambda_0$.

losses, though these states are below the light line so they have a finite radiational lifetime due to the finite length of the chain [see Fig. 6(a)]. When the Bragg condition $\Delta z = 0.5\lambda_f$ is satisfied the spectrum becomes purely Lorentzian, which is defined by the existing highly radiative state of the atomic system, and the main channel is backscattering into the guided mode, propagating in the direction opposite the incident.

The scattering process for $K < 2k_0$ goes through the umklapp process, as shown in Fig. 6(b) by the dashed purple arrow, and corresponds to a vacuum diffraction with a specific k_z. The scattering spectrum acquires a constant region in its central part, with the oscillatory features at the edges as shown in Fig. 8. A further increase in the chain period results in an almost-periodic change in the normalized scattering loss spectra, and, in particular, when $\Delta z = \lambda_f$ ($K = k_f$) we have a Bragg condition of the second order and backscattering into the guided mode with $k_z = -k_f$.

C. Collective coupling of eigenmodes

As pointed out before, the presence of a nanofiber leads to long-range coupling through the guided mode, and with increasing period Δz the features of dispersions and radiation losses near the fiber-mode line are preserved (Figs. 6 and 7). The long-range coupling makes the observed effects purely collective, which results in an increased coupling strength between the collective mode and the guided mode with an increasing number of two-level systems. In particular, the amplitudes of radiation losses peak, related to the imaginary part of the eigenfrequencies, and the splitting of the collective state energy, related to the real part of eigenfrequencies, are shown in Fig. 9 for different numbers of atoms in the chain. One can see that the resonant features becomes more pronounced for larger total numbers of emitters N.

V. DISCUSSION

The normalized scattering loss spectra plotted in Fig. 8 have two qualitatively distinct profiles: (i) a Lorentzian shape profile if the condition of the fiber Bragg diffraction is satisfied [see Figs. 8(b) and 8(e)] and (ii) a profile with a notch in the middle of the spectrum [see Figs. 8(a), 8(c), 8(d), and 8(f)]. The Bragg diffraction is associated with the scattering on the highly radiative state which appears at the edge of the band, similarly to the case shown in Fig. 5. The incident photon is scattered by the radially oriented dipole moment back into the guided mode of the nanofiber. However, for the other periods the photon is diffracted in the cone with a fixed angle, defined by the condition $k_z = k_f - K$ as shown schematically in the right column in Fig. 8.

We associate the change in the spectrum shape with the switching of the diffraction from symmetric (in the case of diffraction into the fiber mode) to asymmetric (diffraction into the vacuum modes) scattering. Asymmetry in photon emission by an excited atom in the vicinity of a nanofiber has been actively discussed recently [38–40]. In particular, it was shown [38] that an atom with transversal and longitudinal components of the dipole moment has asymmetry in forward and backward spontaneous emission rate into the nanofiber mode. This results in asymmetry of the single-atom reflectance of the wave-guding mode propagating in the forward or backward direction, also known as the spin-locking effect [10]. On account of this, in the case of an asymmetric emission rate the Bragg reflection is suppressed and a notched reflectance spectrum [38] is observed. The asymmetry in the case shown in Figs. 8(a), 8(c), 8(d), and 8(f) can be explained by the

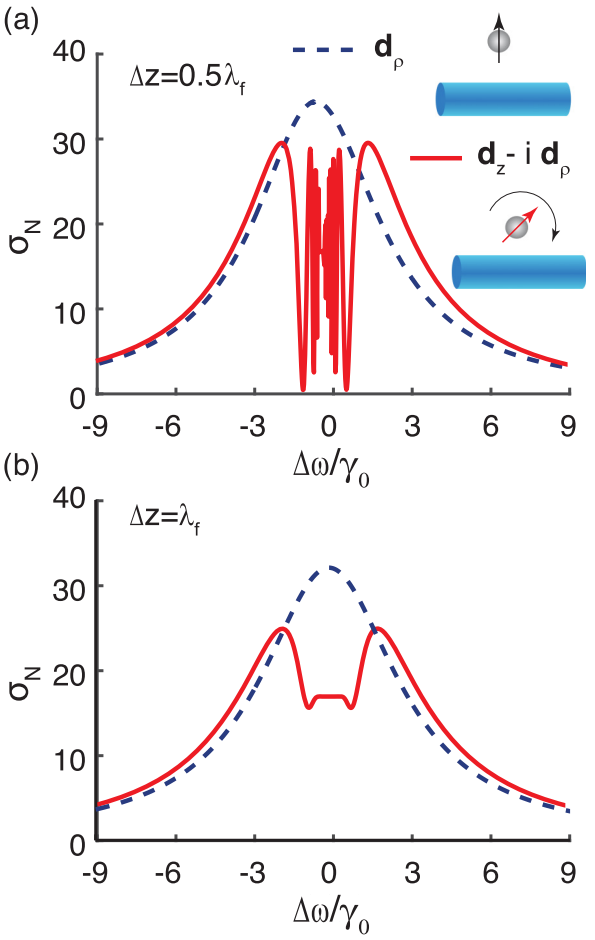

FIG. 10. Normalized scattering loss spectra of the atomic chain consisting of $N = 200$ atoms with radially polarized (dashed line) and σ_+ polarized dipole moments (solid red line) in the regime of (a) the first ($\Delta z = 0.5\lambda_f$) and (b) the second ($\Delta z = \lambda_f$) fiber Bragg diffraction. Parameters are the same as in Fig. 8.

asymmetry in the emission rate of the collective polaritonic states into the vacuum and fiber mode. When the scattering goes back into the fiber mode exactly at the Bragg resonance the symmetry is conserved, but at the vacuum diffraction this symmetry breaks. To support this statement we compared scattering of the incident photon on atoms with (i) a radial component of the dipole moment $\mathbf{d_0}$ and (ii) a σ_+ polarized dipole having both a radial $\mathbf{d}_\rho$ and a z component $\mathbf{d}_z$. In the latter case the two components have $\pi/2$ phase shift but the absolute dipole moment equals $|\mathbf{d}_\rho - i\mathbf{d}_z|/\sqrt{2} = d_0$. Contrary to the radially polarized atom the σ_+ atom has thea strong asymmetry in coupling with the forward- and backward-propagating fiber mode [41]. We have made the calculation for the fiber backscattering regime, where the symmetry should be conserved for the linearly polarized atom but not for the circularly polarized atom. In Fig. 10 the normalized scattering loss spectra are shown for the case of the first and second fiber Bragg resonance in the case of radially polarized atoms (dashed line) and in the case of σ_+ atoms. We see pronounced switching from the Lorentzian spectral shape to a notched shape. For the first fiber Bragg condition $\Delta z = 0.5\lambda_f$ [see Fig. 10(a)], one can see sharp peaks in the center of the band due to scattering by the long-lived collective atomic states. In the case of the second Bragg resonance [see Fig. 10(b)] the sharp peaks are smeared out as all the polaritonic states are above the light cone and, thus, have high losses.

VI. CONCLUSIONS

In this work we have considered a single photon scattering on an ordered finite chain of two-level atoms embedded in a vacuum or trapped in the vicinity of a single-mode dielectric nanofiber. We have developed the scattering matrix technique and analyzed the normalized scattering loss spectrum of a single photon in the presence of a nanofiber. This approach allows us to incorporate the atomic dipole-dipole interactions both via vacuum near fields and via long-range coupling through the guided mode. To support the results of our simulations we have constructed the polaritonic states of the interacting atomic array both in vacuum and close to the nanofiber, which has not been done before for the type of quantum system considered. The obtained dispersion curves for the polaritonic states allowed us to interpret the results of the normalized scattering loss calculations and demonstrated the effects of atomic array coupling with a single guided mode of the nanofiber. Finally, we have shown that the photon scattering over an atomic chain in the presence of a nanofiber is influenced by the effects of spin-locking coupling of atoms with nanofiber and vacuum modes. The proposed approach, which combines construction of the polaritonic eigenstates of the atomic system with the quantum scattering theory, can be effectively applied to modeling experiments on the light interaction with quantum systems at the nanoscale level.

ACKNOWLEDGMENTS

This work was supported by Russian Ministry of Science and Education Project No. RFMEFI58416X0018. M.I.P. acknowledges support from Academy of Finland Grant No. 288591. A.S.S. acknowledges the ITMO Fellowship and Visiting Professorship Program for financial support.

APPENDIX: GREEN'S TENSOR

In order to obtain the Σ^{mn} matrix elements we need to construct the Green's tensor of the system, which can be found from

$$\left[-\frac{\omega^2}{c^2}\varepsilon(\mathbf{r},\omega) + \nabla\times\nabla\times\right]\mathbf{G}(\mathbf{r},\mathbf{r}',\omega) = \mathbf{I}\delta(\mathbf{r}-\mathbf{r}'), \quad \text{(A1)}$$

where $\varepsilon(\mathbf{r},\omega)$ is the complex dielectric function and $\mathbf{I}$ is the unit dyad. In our case we consider a dielectric cylindrical wave guide of radius ρ_c and dielectric permittivity ε being constant inside the cylinder. To find the solution we apply the scattering superposition method [35,42], which allows us to expand the Green's tensor into homogeneous and inhomogeneous terms:

$$\mathbf{G}(\mathbf{r},\mathbf{r}',\omega) = \mathbf{G}_0(\mathbf{r},\mathbf{r}',\omega) + \mathbf{G}_s(\mathbf{r},\mathbf{r}',\omega). \quad \text{(A2)}$$

As soon as we consider atomic dipoles in the vicinity of the wave guide, so that $\mathbf{r}$ and $\mathbf{r}'$ are outside the cylinder, the homogeneous term is always present and describes the field generated directly by the source placed at point $\mathbf{r}'$ at field point $\mathbf{r}$. This term can be obtained analytically from the Green tensor written in Cartesian coordinates using the transformation from Cartesian to cylindrical coordinates $\mathbf{S}(\phi)\mathbf{G}_0^{\mathrm{Cart}}(\mathbf{r},\mathbf{r}',\omega)\mathbf{S}^T(\phi)$, where $\mathbf{G}_0^{\mathrm{Cart}}$ has an analytic expression [43] and is given by

$$\mathbf{G}_0^{\mathrm{Cart}}(\mathbf{r},\mathbf{r}',\omega) = \left(\mathbf{I} + \frac{1}{k^2}\nabla\otimes\nabla\right)G_0(\mathbf{r},\mathbf{r}',\omega), \quad \text{(A3)}$$

where $G_0(\mathbf{r},\mathbf{r}',\omega)$ is the Green's function of the scalar Helmholtz equation.

The scattering term can be calculated via the integral representation of the homogeneous part. To obtain this representation we apply the method of VWF explained in detail in Refs. [44] and [45]; here we cover only the basic ideas and provide the final expressions. To find the solution of the vector Helmholtz equation, (A1), we introduce the scalar Helmholtz equation and the solution of this equation in the cylindrical coordinates,

$$\nabla^2\phi(\mathbf{k},\mathbf{r}) + k^2\phi(\mathbf{k},\mathbf{r}) = 0,$$
$$\phi_n(k_z,\mathbf{r}) = J_n(k_\rho\rho)e^{in\theta+ik_z z}, \quad \text{(A4)}$$

where $J_n(x)$ is the Bessel function of the first kind, $\mathbf{r} = (\rho,\theta,z)$ are the cylindrical coordinates, and k_ρ and k_z are the projections of the wave vector $\mathbf{k}$. The solution of the vector Helmholtz equation may be written in terms of the vector wave functions

$$\mathbf{M}_n(k_z,\mathbf{r}) = \nabla\times[\phi_n(k_z,\mathbf{r})\mathbf{e_z}],$$
$$\mathbf{N}_n(k_z,\mathbf{r}) = \frac{1}{k}\nabla\times\mathbf{M}_n(k_z,\mathbf{r}), \quad \text{(A5)}$$

where $\mathbf{e_z}$ is the so-called pilot vector, the unit vector pointing in the z direction. These WVFs $\mathbf{M}$ and $\mathbf{N}$ correspond to TE/TM modes of the field.

One can show [44] that the homogeneous part of the Green's function can be expanded in terms of these vector

wave functions as

$$\mathbf{G}_h(\mathbf{r},\mathbf{r}',\omega) = -\frac{\mathbf{e}_\rho\mathbf{e}_\rho}{k_0^2}\delta(\mathbf{r}-\mathbf{r}') + \frac{i}{8\pi}\sum_{n=-\infty}^{\infty}\int_{-\infty}^{\infty}\frac{dk_z}{k_{0\rho}^2}\mathbf{F}_n(k_z,\mathbf{r},\mathbf{r}'), \quad \text{(A6)}$$

and the $\mathbf{F}_n(k_z,\mathbf{r},\mathbf{s})$ function is given by

$$\mathbf{M}_n^{(1)}(k_z,\mathbf{r})\overline{\mathbf{M}}_n(k_z,\mathbf{r}') + \mathbf{N}_n^{(1)}(k_z,\mathbf{r})\overline{\mathbf{N}}_n(k_z,\mathbf{r}'),$$

$$\mathbf{M}_n(k_z,\mathbf{r})\overline{\mathbf{M}}_n^{(1)}(k_z,\mathbf{r}') + \mathbf{N}_n(k_z,\mathbf{r})\overline{\mathbf{N}}_n^{(1)}(k_z,\mathbf{r}').$$

Here the first line holds for $\rho_r > \rho_{r'}$ and the second one for $\rho_r < \rho_{r'}$; $k_0 = \omega/c$, $k_{0\rho} = \sqrt{k_0^2 - k_z^2}$, and the superscript (1) in vector wave functions denotes that the Bessel function of the first kind, $J_n(k_\rho\rho)$, should be replaced with the Hankel function of the first kind, $H_n^{(1)}(k_\rho\rho)$. Here we provide the explicit form of the WVF:

$$\mathbf{M}_n(k_z,\mathbf{r}) = \begin{pmatrix} \frac{in}{\rho}J_n(k_{0\rho}\rho) \\ -k_{0\rho}(J_n(k_{0\rho}\rho))' \\ 0 \end{pmatrix} e^{in\theta+ik_zz},$$

$$\mathbf{N}_n(k_z,\mathbf{r}) = \begin{pmatrix} \frac{ik_zk_{0\rho}}{k}(J_n(k_{0\rho}\rho))' \\ -\frac{nk_z}{\rho k}J_n(k_{0\rho}\rho) \\ \frac{k_{0\rho}^2}{k}J_n(k_{0\rho}\rho) \end{pmatrix} e^{in\theta+ik_zz},$$

$$\overline{\mathbf{M}}_n(k_z,\mathbf{r}') = \begin{pmatrix} -\frac{in}{\rho'}J_n(k_{0\rho}\rho') \\ -k_{0\rho}(J_n(k_{0\rho}\rho'))' \\ 0 \end{pmatrix}^T e^{-in\theta'-ik_zz'},$$

$$\overline{\mathbf{N}}_n(k_z,\mathbf{r}') = \begin{pmatrix} -\frac{ik_zk_{0\rho}}{k}(J_n(k_{0\rho}\rho'))' \\ -\frac{nk_z}{\rho'k}J_n(k_{0\rho}\rho') \\ \frac{k_{0\rho}^2}{k}J_n(k_{0\rho}\rho') \end{pmatrix}^T e^{-in\theta'-ik_zz'},$$

where $J_n(k_\rho\rho)'$ indicates the derivative with respect to the dimensionless argument.

Now having the integral representation of the homogeneous term of the Green's function, we can construct the scattering term in a similar fashion. Let us denote the medium outside the dielectric cylinder 1 and the medium inside 2. The particular form of the Green's tensor depends on the position of the source point $\mathbf{r}'$: whether it is inside or outside the cylinder. Since the atoms are placed outside the nanofiber, both source and receiver should be outside the cylinder, and in the latter we consider only the second case. Thus, the total Green's tensor can be written as

$$\mathbf{G}^{11}(\mathbf{r},\mathbf{r}',\omega) = \mathbf{G}_h^{11}(\mathbf{r},\mathbf{r}',\omega) + \mathbf{G}_s^{11}(\mathbf{r},\mathbf{r}',\omega),$$

$$\mathbf{G}^{21}(\mathbf{r},\mathbf{r}',\omega) = \mathbf{G}_s^{21}(\mathbf{r},\mathbf{r}',\omega),$$

where the two superscripts denote the positions of the receiver and the source point, respectively, and the two scattering parts of the Green's tensor have the following form:

$$\mathbf{G}_s^{11}(\mathbf{r},\mathbf{r}',\omega) = \frac{i}{8\pi}\sum_{n=-\infty}^{\infty}\int_{-\infty}^{\infty}\frac{dk_z}{k_{\rho1}^2}\mathbf{F}_{\mathbf{M};n,1}^{11(1)}(k_z,\mathbf{r})\overline{\mathbf{M}}_{n,1}^{(1)}(k_z,\mathbf{r}') + \mathbf{F}_{\mathbf{N};n,1}^{11(1)}(k_z,\mathbf{r})\overline{\mathbf{N}}_{n,1}^{(1)}(k_z,\mathbf{r}'),$$

$$\mathbf{F}_{\mathbf{M};n,1}^{11(1)}(k_z,\mathbf{r}) = R_{MM}^{11}\mathbf{M}_{n,1}^{(1)}(k_z,\mathbf{r}) + R_{NM}^{11}\mathbf{N}_{n,1}^{(1)}(k_z,\mathbf{r}),$$

$$\mathbf{F}_{\mathbf{N};n,1}^{11(1)}(k_z,\mathbf{r}) = R_{MN}^{11}\mathbf{M}_{n,1}^{(1)}(k_z,\mathbf{r}) + R_{NN}^{11}\mathbf{N}_{n,1}^{(1)}(k_z,\mathbf{r}),$$

$$\mathbf{G}_s^{21}(\mathbf{r},\mathbf{r}',\omega) = \frac{i}{8\pi}\sum_{n=-\infty}^{\infty}\int_{-\infty}^{\infty}\frac{dk_z}{k_{\rho1}^2}\mathbf{F}_{\mathbf{M};n,2}^{21}(k_z,\mathbf{r})\overline{\mathbf{M}}_{n,1}^{(1)}(k_z,\mathbf{r}') + \mathbf{F}_{\mathbf{N};n,1}^{21}(k_z,\mathbf{r})\overline{\mathbf{N}}_{n,1}^{(1)}(k_z,\mathbf{r}'),$$

$$\mathbf{F}_{\mathbf{M};n,2}^{21}(k_z,\mathbf{r}) = R_{MM}^{21}\mathbf{M}_{n,2}(k_z,\mathbf{r}) + R_{NM}^{21}\mathbf{N}_{n,2}(k_z,\mathbf{r}),$$

$$\mathbf{F}_{\mathbf{N};n,2}^{21}(k_z,\mathbf{r}) = R_{MN}^{21}\mathbf{M}_{n,2}(k_z,\mathbf{r}) + R_{NN}^{21}\mathbf{N}_{n,2}(k_z,\mathbf{r}).$$

Here the scattering Fresnel coefficients R_{AB}^{ij} are introduced and the second subscript in the VWFs denotes that k and k_ρ should be replaced with their values inside the corresponding media $k_i = \varepsilon_i(\mathbf{r},\omega)k_0$, $k_{\rho i} = \sqrt{k_i^2 - k_z^2}$. We should note that unlike the case of the homogeneous term, here we have products of $\mathbf{M}$ and $\mathbf{N}$, which is due to the fact that the normal modes in our case have a hybrid nature.

The form of the Fresnel coefficients mentioned above can be found by imposing the boundary conditions on the Green's tensor at the surface of the cylinder:

$$\mathbf{e}_\rho \times [\mathbf{G}^{11}(\mathbf{r},\mathbf{r}',\omega) - \mathbf{G}^{21}(\mathbf{r},\mathbf{r}',\omega)]|_{\rho_r=\rho_c} = 0,$$

$$\mathbf{e}_\rho \times \nabla_\mathbf{r} \times [\mathbf{G}^{11}(\mathbf{r},\mathbf{r}',\omega) - \mathbf{G}^{21}(\mathbf{r},\mathbf{r}',\omega)]|_{\rho_r=\rho_c} = 0.$$

Solving for this, we can find the Fresnel coefficients R_{AB}^{ij} and, finally, construct the scattering part of the Green's tensor $\mathbf{G}_s(\mathbf{r},\mathbf{r}',\omega)$.

[1] H. J. Kimble, Nature **453**, 1023 (2008).

[2] A. V. Akimov, A. Mukherjee, C. L. Yu, D. E. Chang, A. S. Zibrov, P. R. Hemmer, H. Park, and M. D. Lukin, Nature **450**, 402 (2007).

[3] H. de Riedmatten, M. Afzelius, M. U. Staudt, C. Simon, and N. Gisin, Nature **456**, 773 (2008).

[4] S. J. Weber, A. Chantasri, J. Dressel, A. N. Jordan, K. W. Murch, and I. Siddiqi, Nature **511**, 570 (2014).

[5] P. J. Yao, V. Manga Rao, and S. Hughes, Laser Photon. Rev. **4**, 499 (2010).

[6] P. Lodahl, S. Mahmoodian, and S. Stobbe, Rev. Mod. Phys. **87**, 347 (2015).

[7] L. M. Duan and C. Monroe, Adv. At. Mol. Opt. Phys. **55**, 419 (2008).

[8] K. M. Birnbaum, A. Boca, R. Miller, A. D. Boozer, T. E. Northup, and H. J. Kimble, Nature **436**, 87 (2005).

[9] N. Rivera, I. Kaminer, B. Zhen, J. D. Joannopoulos, and M. Soljačić, Science **353**, 263 (2016).

[10] K. Y. Bliokh, D. Smirnova, and F. Nori, Science (N.Y.) **348**, 1448 (2015).

[11] S. J. P. Kress, F. V. Antolinez, P. Richner, S. V. Jayanti, D. K. Kim, F. Prins, A. Riedinger, M. P. C. Fischer, S. Meyer, K. M. McPeak, D. Poulikakos, and D. J. Norris, Nano Lett. **15**, 6267 (2015).
[12] R. J. Coles, D. M. Price, J. E. Dixon, B. Royall, E. Clarke, P. Kok, M. S. Skolnick, A. M. Fox, and M. N. Makhonin, Nat. Commun. **7**, 11183 (2016).
[13] F. L. Kien, J. Q. Liang, K. Hakuta, and V. I. Balykin, Opt. Commun. **242**, 445 (2004).
[14] K. P. Nayak, P. N. Melentiev, M. Morinaga, F. L. Kien, V. I. Balykin, and K. Hakuta, Opt. Express **15**, 5431 (2007).
[15] E. Vetsch, D. Reitz, G. Sagué, R. Schmidt, S. T. Dawkins, and A. Rauschenbeutel, Phys. Rev. Lett. **104**, 203603 (2010).
[16] V. I. Balykin, K. Hakuta, F. Le Kien, J. Q. Liang, and M. Morinaga, Phys. Rev. A **70**, 011401(R) (2004).
[17] M. S. Tame, K. R. McEnery, S. K. Özdemir, J. Lee, S. A. Maier, and M. S. Kim, Nat. Phys. **9**, 329 (2013).
[18] P. Törmä and W. L. Barnes, Rep. Prog. Phys. **78**, 013901 (2015).
[19] W. H. Weber and G. W. Ford, Phys. Rev. B **70**, 125429 (2004).
[20] S. Campione, S. Steshenko, and F. Capolino, Opt. Express **19**, 18345 (2011).
[21] M. Petrov, Phys. Rev. A **91**, 023821 (2015).
[22] R. S. Savelev, D. S. Filonov, M. I. Petrov, A. E. Krasnok, P. A. Belov, and Y. S. Kivshar, Phys. Rev. B **92**, 155415 (2015).
[23] F. Le Kien and A. Rauschenbeutel, Phys. Rev. A **90**, 063816 (2014).
[24] F. Le Kien, S. Dutta Gupta, V. I. Balykin, and K. Hakuta, Phys. Rev. A **72**, 032509 (2005).
[25] L. Russell, D. A. Gleeson, V. G. Minogin, and S. N. Chormaic, J. Phys. B **42**, 185006 (2009).
[26] H. L. Sørensen, J.-B. Béguin, K. W. Kluge, I. Iakoupov, A. S. Sørensen, J. H. Müller, E. S. Polzik, and J. Appel, Phys. Rev. Lett. **117**, 133604 (2016).
[27] N. V. Corzo, B. Gouraud, A. Chandra, A. Goban, A. S. Sheremet, D. V. Kupriyanov, and J. Laurat, Phys. Rev. Lett. **117**, 133603 (2016).
[28] A. Goban, K. S. Choi, D. J. Alton, D. Ding, C. Lacroûte, M. Pototschnig, T. Thiele, N. P. Stern, and H. J. Kimble, Phys. Rev. Lett. **109**, 033603 (2012).
[29] C. Cohen-Tannoudji, J. Dupont-Roc, and G. Grynberg, *Photons and Atoms: Introduction to Quantum Electrodynamics* (Wiley-VCH Verlag, Weinheim, Germany, 2004).
[30] A. S. Sheremet, A. D. Manukhova, N. V. Larionov, and D. V. Kupriyanov, Phys. Rev. A **86**, 043414 (2012).
[31] V. M. Ezhova, L. V. Gerasimov, and D. V. Kupriyanov, J Phys.: Conf. Ser. **769**, 012045 (2016).
[32] V. G. Minogin and S. Nic Chormaic, Laser Phys. **20**, 32 (2010).
[33] T. Gruner and D.-G. Welsch, Phys. Rev. A **53**, 1818 (1996).
[34] H. T. Dung, L. Knöll, and D.-G. Welsch, Phys. Rev. A **66**, 063810 (2002).
[35] C. A. Marocico and J. Knoester, Phys. Rev. A **79**, 053816 (2009).
[36] R. S. Savelev, A. P. Slobozhanyuk, A. E. Miroshnichenko, Y. S. Kivshar, and P. A. Belov, Phys. Rev. B **89**, 035435 (2014).
[37] V. Agranovich and O. Dubovsky, JETP Lett. **3**, 223 (1966).
[38] F. Le Kien and A. Rauschenbeutel, Phys. Rev. A **91**, 053847 (2015).
[39] C. Junge, D. O'Shea, J. Volz, and A. Rauschenbeutel, Phys. Rev. Lett. **110**, 213604 (2013).
[40] R. Mitsch, C. Sayrin, B. Albrecht, P. Schneeweiss, and A. Rauschenbeutel, Nat. Commun. **5**, 5713 (2014).
[41] T. Van Mechelen and Z. Jacob, Optica **3**, 118 (2016).
[42] C. A. Marocico and J. Knoester, Phys. Rev. A **84**, 053824 (2011).
[43] L. Novotny and B. Hecht, *Principles of Nano-Optics* (Cambridge University Press, Cambridge, UK, 2012).
[44] W. C. Chew, *Waves and Fields in Inhomogeneous Media* (Wiley-IEEE Press, New York, 1999).
[45] C. T. Tai, *Dyadic Green's Functions in Electromagnetic Theory*, 2nd ed. (IEEE Press, Piscataway, NJ, 1994).